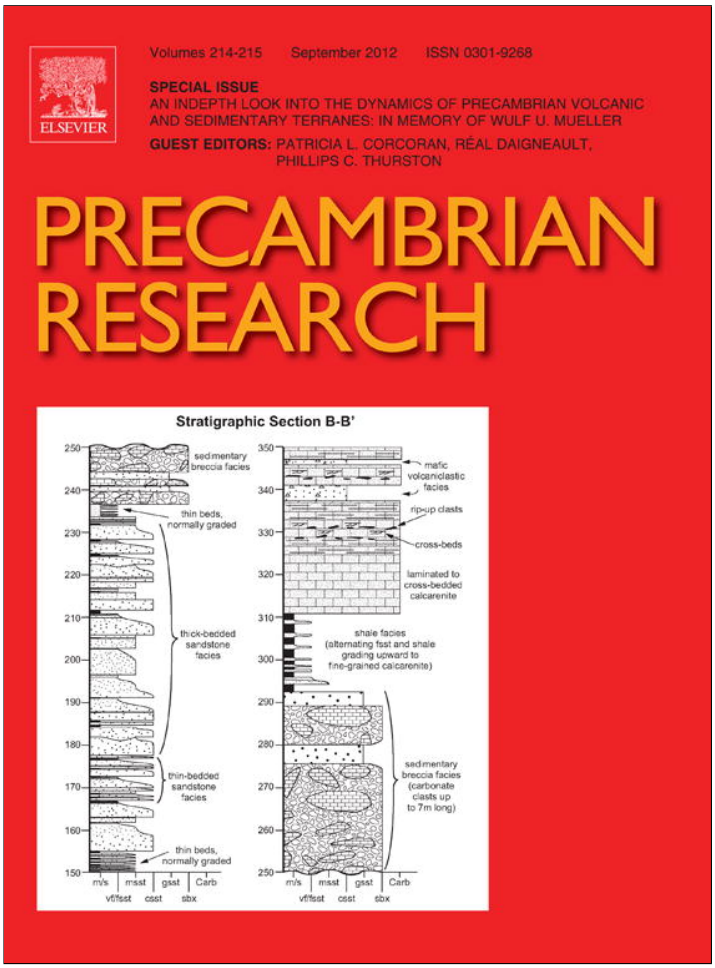

Precambrian Research 214–215 (2012) 258–268

Contents lists available at SciVerse ScienceDirect

Precambrian Research

journal homepage: www.elsevier.com/locate/precamres

Ion microprobe analyses of $\delta^{18}O$ in early quartz cements from 1.9 Ga granular iron formations (GIFs): A pilot study

Lauren C. Cunningham[a], F. Zeb Page[a], Bruce M. Simonson[a,*], Reinhard Kozdon[b], John W. Valley[b]

[a] Department of Geology, Oberlin College, 52 West Lorain Street, Oberlin, OH 44074, USA
[b] NASA Astrobiology Institute, WiscSIMS, Department of Geoscience, University of Wisconsin, Madison, Madison, WI 53706, USA

ARTICLE INFO

Article history:
Received 1 August 2011
Received in revised form 19 January 2012
Accepted 23 January 2012
Available online 2 February 2012

Keywords:
Oxygen isotopes
Gunflint Iron Formation
Sokoman Iron Formation
Cathodoluminescence
Ion microprobe
Quartz diagenesis

ABSTRACT

The low $\delta^{18}O$ values of Precambrian cherts have been widely used to infer that temperatures were higher and/or seawater $\delta^{18}O$ was lower compared to today's oceans. However, the Precambrian cherts presented as evidence for these temperatures are neomorphosed from amorphous precursors that originally precipitated from ocean water, suggesting diagenetic alteration is an important cause of the widespread low-$\delta^{18}O$ values. Many pores between sand-size clasts in granular iron formations (GIFs) are filled with coarsely crystalline quartz cements that are texturally primary. In unmetamorphosed GIF samples from the 1.9 Ga Gunflint and Sokoman iron formations, synsedimentary clasts of GIF and high minus-cement porosities (the volume of pore space occupied by recognizable cement, inversely proportional to the degree of compaction) indicate such cements precipitated directly from pore water near the depositional interface. Growth bands identified in quartz cement crystals using cathodoluminescence (CL) imaging further confirm their void-filling and unrecrystallized nature. In order to test the effect of neomorphism on the $\delta^{18}O$ of silica in these rocks, unrecrystallized primary quartz cements and neomorphic quartz in adjacent clasts were both analyzed by ion microprobe. Values of $\delta^{18}O$ range from 23.5 to 26.4‰ VSMOW in cements and 21.3–26.8‰ in clasts in samples from the Gunflint Iron Formation. Samples from the Sokomon Iron Formation record deeper, more evolved pore waters and in some cases contain lower $\delta^{18}O$ cements. In individual pores of Gunflint samples, cement values vary only slightly more than analytical uncertainty from edge to center and no consistent increasing or decreasing trends were observed. Overall, the $\delta^{18}O$ of the cements are similar to the most elevated $\delta^{18}O$ reported from cherts of similar age, but span a substantially smaller range. This suggests most of the lower values reported previously reflect late-diagenetic conditions at greater burial depths. The shallow, possibly restricted seas above the Gunflint and Sokoman GIFs appear to have been warmer and may have been lower in $\delta^{18}O$ than present-day seawater, but they may not have been representative of global seawater.

1. Introduction

The assertion that ocean temperatures in the Precambrian were substantially warmer than they are at present remains a contentious subject. The principal line of evidence for elevated ocean temperatures is the ^{18}O-depleted nature of Archean and Proterozoic cherts, compared to typical modern values (Knauth and Epstein, 1976; Knauth and Lowe, 1978, 2003). Indeed, all analyses of $\delta^{18}O$ from silica phases found in Precambrian cherts are on the order of 10‰ or more depleted in ^{18}O than those found in Phanerozoic samples, and appear to record a secular trend in both $\delta^{18}O$ and $\delta^{30}Si$ (Robert and Chaussidon, 2006).

The $\delta^{18}O$ of silica that forms in equilibrium with a fluid (such as seawater) depends on the $\delta^{18}O$ of the fluid as well as the temperature. For the universally low $\delta^{18}O$ values from silica in iron formations to be unequivocal evidence of high ocean temperatures, three major underlying assumptions must be substantiated: the $\delta^{18}O$ of the water in equilibrium with the cherts at the time of formation must be constrained, the water must be representative of global seawater in terms of temperature and composition, and the isotopic composition of the quartz must represent a primary geochemical signal preserved in Precambrian chemical sediment, unaffected by subsequent neomorphism, recrystallization, or metamorphism. These points have been discussed at length and continue to be matters of debate (see Perry and Lefticariu, 2007, for a review). The powerful buffering effect of a homogeneous mantle oxygen reservoir on seawater through hydrothermal alteration of ocean crust makes a substantial secular change in seawater $\delta^{18}O$ seem unlikely (Muehlenbachs and Clayton, 1976; Karhu and

* Corresponding author. Fax: +1 440 775 8038.
E-mail address: bruce.simonson@oberlin.edu (B.M. Simonson).

0301-9268/$ – see front matter © 2012 Elsevier B.V. All rights reserved.
doi:10.1016/j.precamres.2012.01.016

Epstein, 1986; Muehlenbachs, 1998, 2008). However, the fidelity of the oxygen isotope record preserved in Precambrian cherts remains less clear. In particular, the vast majority of Precambrian chert available for analysis is composed of fine-grained, equigranular α-quartz (sometimes termed microquartz) and chalcedony. Precambrian cherts most likely initially precipitated as amorphous or opaline oozes in equilibrium with a silica-saturated ocean (Knauth, 2005). Therefore, the vast majority of chert $\delta^{18}O$ analyses are based on material that was neomorphosed during diagenesis, providing opportunity for the isotopic record to be modified. Furthermore, many $\delta^{18}O$ analyses of cherts have been made on mg-sized samples mechanically separated from the host-rock allowing for possible analysis of mixed domains in the chert, or for possible contamination by the abundant low-$\delta^{18}O$ magnetite found in iron formation chert. Most recently, ion microprobe studies of quartz have been combined with geochemical modeling and fluid inclusion work to assess the effects of diagenetic and hydrothermal alteration on the preservation of primary $\delta^{18}O$ in Precambrian cherts (Marin et al., 2010; Marin-Carbonne et al., 2011; Heck et al., 2011).

In this study, we analyze a small but carefully selected group of samples to test the hypothesis that a primary oxygen isotope signal can be preserved in silica from an iron formation. Our approach differs from that of previous workers in that we analyzed unrecrystallized primary quartz formed as cement in granular iron formations (GIFs) very early in diagenesis (Simonson, 1987). Previous studies of oxygen isotopes in quartz cements have, to our knowledge, all focused on overgrowth cements in quartzose sandstones (e.g., Lee and Savin, 1985; Pollington et al., 2011). In clastic units like these, the oxygen isotopic values of the framework grains reflect processes in distant source rocks and cements can be dramatically higher in $\delta^{18}O$. In contrast, the framework particles and some cements in iron formations precipitate from waters that are probably closely connected (see Simonson, 1987 and Section 2.3). Our isotopic analyses were guided by petrographic analyses of polished thin sections and took advantage of the extremely high spatial resolution of the ion microprobe. By analyzing unrecrystallized quartz cements formed close to the sediment–water interface, we hope to shed light on the nature of the seawater in iron formation basins.

2. Background information

2.1. Geologic setting

Iron formations contain much of the silica precipitated from seawater in the early Precambrian. Although iron formations are defined on the basis of their content of >15% iron, it is a rare Precambrian iron formation that does not contain a substantial component of chert or its metamorphosed equivalent (Klein, 2005). Iron formations disappeared almost entirely from the stratigraphic record after ~1.8 Ga, most likely as a result of linked secular changes in Earth's atmosphere, hydrosphere, biosphere, and lithosphere (Bekker et al., 2010). Given the sheer mass of chert in iron formations as well as the textures they display (Maliva et al., 2005), the silica in most iron formations is generally believed to be a primary component.

A first-order question in the preservation of primary $\delta^{18}O$ in Precambrian cherts is the possibility of alteration through neomorphism, recrystallization, or intracrystalline diffusion during subsequent metamorphism. Although quartz has relatively slow intracrystalline diffusion rates for oxygen under sedimentary or diagenetic conditions (e.g., Jones and Knauth, 1979; Cole and Chakraborty, 2001), recrystallization and diffusion are common under medium- to high-grade metamorphic conditions and it is not typically retentive of $\delta^{18}O$ (e.g., Sharp et al., 1991; Valaas Hyslop et al., 2008). To minimize the potential for resetting by neomorphism or metamorphic diffusion, samples for this pilot study were chosen from two iron formations where they experienced little or no metamorphism: the Gunflint Iron Formation near Thunder Bay, Ontario (Floran and Papike, 1975), and the Sokoman Iron Formation near Schefferville, Quebec (Zajac, 1974). Both of these iron formations were deposited around 1.9 Ga.

While it is highly deformed and metamorphosed in many parts of the Labrador Trough, the Sokoman Iron Formation in the Howells River area ~10 km southwest of the town of Schefferville is nearly flat-laying and essentially unmetamorphosed (Klein, 1978). Klein and Fink (1976) concluded that the maximum diagenetic temperature reached in the Howells River area was 150 °C. Likewise, where the Gunflint Iron Formation was sampled in Ontario, it is nearly flat-lying and essentially unmetamorphosed. Without specifying any maximum diagenetic temperatures, Floran and Papike (1975, p. 1169) argue that the iron silicates in the Gunflint Iron Formation could have formed at temperatures of <100 °C. Extremely low levels of metamorphic or even diagenetic alteration are also evidenced by the presence of well-preserved microfossils in both the Gunflint (Awramik and Barghoorn, 1977) and Sokoman (Knoll and Simonson, 1981) Iron Formations in the areas sampled.

2.2. Why focus on granular instead of banded iron formations?

The two main textural types of iron formations are banded (BIF) and granular (GIF) (see Bekker et al., 2010 for a recent review). BIFs are laminated, fine-grained chemical muds deposited in deeper water whereas GIFs are coarser-grained and originated as chemical sands (Fig. 1) in higher energy, shallower shelf environments. Most iron formations are marine in origin, but the paleoenvironments in which they accumulated were probably not typical of open-marine conditions. Because of their coarser original grain size, primary clasts and cements are easier to identify in GIFs than in BIFs. Specifically, most GIFs consist of well-sorted sand-size iron- and silica-rich clasts (peloids, ooids and/or intraclastic grains) with intergranular pores on the order of 0.5 mm across. Most of the cement filling the pores in GIFs consists of drusy to blocky quartz (Fig. 2A), chalcedony (radial- to parallel-fibrous cements) (Fig. 2B), and/or chert (Simonson, 1987). In contrast, original clasts and secondary pore fillings cannot be distinguished from one another petrographically in BIFs because the original intergranular pores were so small. Much of the silica cement in both GIFs and BIFs was emplaced early in diagenesis based on differential compaction around silica-rich pods or zones (Simonson, 2003; Beukes and Gutzmer, 2008). More specific evidence that some cements in GIFs were emplaced very early is outlined in the next section.

2.3. Sedimentary textures and sample selection

The sedimentary textures of GIFs have been examined extensively (e.g., Dimroth and Chauvel, 1973; Floran and Papike, 1975; Simonson, 1987) and have properties typical of any sediment consisting of well-sorted sand grains. For example, a well-sorted framework of equant clasts typically has ~40% intergranular depositional porosity whether it consists of carbonate ooids (Enos and Sawatsky, 1981), quartzose sand (Beard and Weyl, 1973), or peloids of iron and silica. Another property of well-sorted, uncompacted sand of equant clasts is that a given grain on average shows only ~1 contact with a neighboring grain in a random two-dimensional cross-section. In a similar sand that has been highly compacted, each clast shows ~5 contacts with neighboring clasts in a random cross-section (Pettijohn, 1975, p. 75). Intergranular pores can be eliminated during diagenesis through cementation as well as compaction; GIFs show good examples of both (Simonson, 1987). As

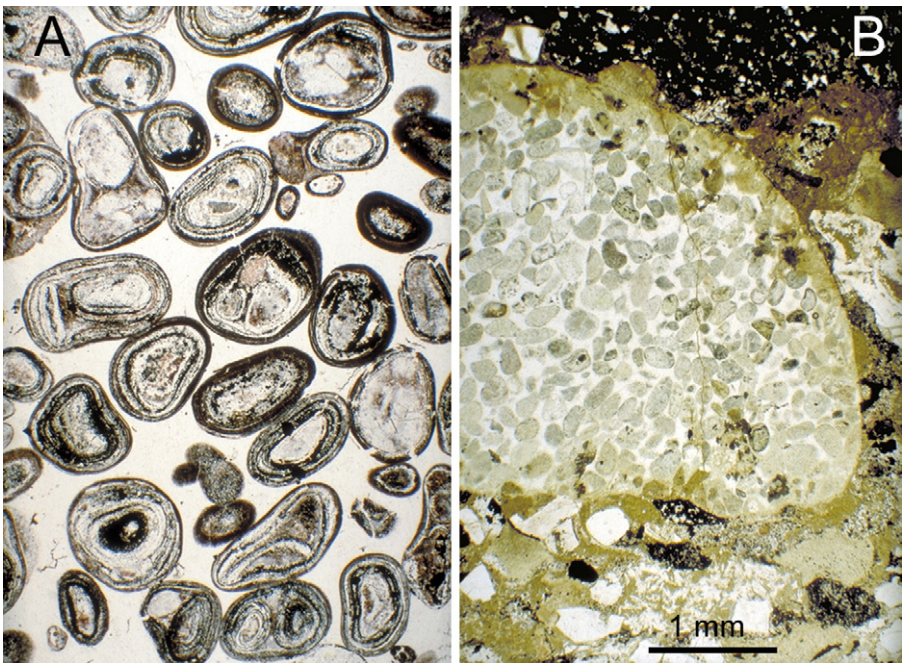

Fig. 1. Photomicrographs in plane polarized light of GIFs from the Sokoman Iron Formation viewed at the same magnification. (A) Well-sorted framework of chert–hematite oolites. This GIF consists of 66% clasts and 34% cement (clear quartz and chert) by volume with virtually no residual open pore space. (B) A pebble of GIF in a conglomeratic bed deposited by an unusually high energy event. The pebble consists of well-sorted chert–silicate peloids with 29% intergranular quartz and chert cement (clear) by volume. The smooth, well-rounded upper edge of the pebble indicates the cements and peloids were abraded together. The sediment surrounding the pebble is a mix of volcaniclastic detritus (including clear quartz and cloudy feldspar grains) and iron formation intraclasts (including opaque iron oxide-rich flat pebble at top and greenish iron silicates).

noted above, most of the intergranular cements in unmetamorphosed GIFs consist of silica polymorphs (Fig. 2).

Multiple characteristics of GIFs suggest that some silica cements precipitated very close to the sediment–water interface in uncompacted sediment. One such characteristic is the high minus-cement porosities of many GIFs (Fig. 1A). Minus-cement porosity is the volume of pore space equivalent to what is currently occupied by recognizable cement in lithified sediment. Some GIFs have minus-cement porosities as high as 41% (Simonson, 1987); since this is equal to the depositional porosity of well-sorted sands, it requires at least some cementation prior to significant burial to prevent compaction. Such GIFs also show the low number of contacts per grain to be expected with minimal compaction. The presence of rare intraclasts of cemented GIF incorporated into high-energy interbeds in GIFs (Fig. 1B) also requires synsedimentary cementation. Fine-grained sediments like BIFs are naturally more cohesive than sands. Most of the peloids and flat pebbles in GIFs are interpreted as intraformational rip-up clasts, but sand grains do not adhere to one another to form intraclasts unless they are cemented prior to erosion or otherwise bound together, e.g., by microbial mats. The presence of GIF intraclasts in both the Gunflint and Sokoman Iron Formations (Simonson, 1987) signals some silica cementation within reach of erosion, presumably no more than a meter or so below the sediment–water interface. A third characteristic of GIFs requiring early cementation are vertical cracks and subhorizontal vugs that are filled with a combination of fine sediment and cement (Fig. 3). The fact that the edges of the cracks and vugs cut across both clasts and cements indicates these voids formed after the cements were already in place; their formation close to the sediment–water interface is demonstrated by the presence of cross-laminated internal sediment and rip-up clasts in some vugs and cracks. The septarian geometry of some of the cracks suggests they formed via syneresis (shrinkage during the dewatering of silica gel precursor sediment and cement) and also implies at least some of the chert is primary rather than replaced carbonate (Simonson, 1987; Maliva et al., 2005). Carbonate is present in many GIFs, but typically as crystals replacing silica phases rather than vice versa. A fourth line of evidence suggesting some silica cements formed very close to the sediment–water interface is the presence of stromatolites cored with silica-cemented GIFs. A free surface on loose, water-saturated sands cannot exceed the angle of repose, yet some of the contacts between stromatolitic laminations and GIFs are vertical or even overturned with no evidence of soft-sediment deformation. This suggests some stromatolites grew on erosion surfaces on sands that had been previously stabilized via cementation.

For our study, we selected samples with the highest probability of containing cements formed very close to the sediment–water interface. One criterion was their high minus-cement porosity, suggesting minimal compaction prior to cementation; such samples also contain the largest cement crystals (Figs. 1–3). Cement crystals begin by nucleating on the surfaces of sediment grains. As the crystals grow larger they begin to fill the pore, crowding each other out, a process Grigor'ev (1965) termed 'geometrical selection'. This competition ensures that the smallest crystals will be located along the edges of ooids and peloids whereas the more favorably oriented crystals that grow outwards faster become larger crystals filling the centers of the voids (Fig. 2A); this is known as a drusy texture. As crystal growth occludes the pores, new growth bands common to all crystals are added. Sometimes growth planes are visible in plane polarized light due to fluid or other minute inclusions trapped on crystal facets during pauses or rapid accelerations in crystal growth; such features are known as veils (Fig. 3). The center of the pore is often distinguishable as the site where crystals growing from many different directions meet. Druse is the ideal cement type as it is coarsely crystalline and indicates both void-filling precipitation and a lack of recrystallization. Furthermore, large drusy crystals are an excellent place to study variation in chemical composition over time. We therefore selected four samples with drusy cements for analysis in our study (see Section 4 for details).

The high surface-area to volume ratio of chalcedony may make it less likely than druse to preserve primary isotopic signatures.

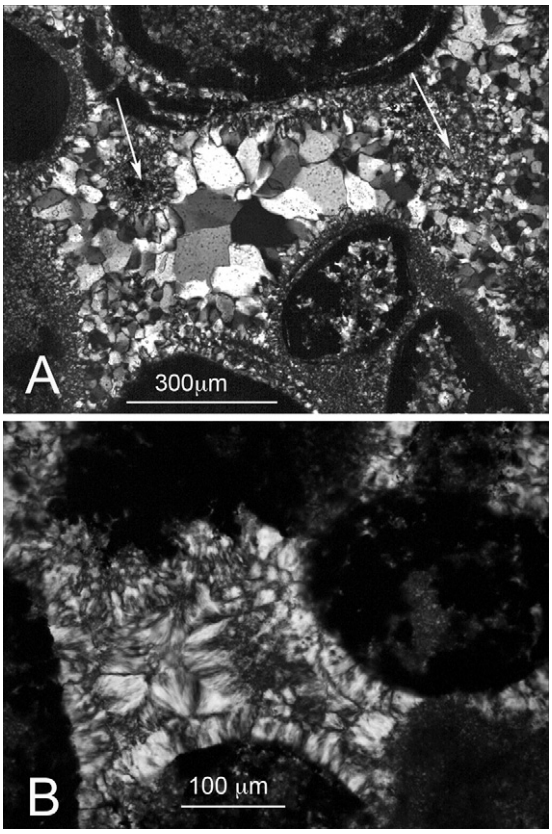

Fig. 2. Photomicrographs (with crossed polarizers) of void-filling cements in GIFs. (A) Quartz druse in typical pore between ooids; finer chert-like clots in middle of pores (arrows) are probably tangential cuts through tips of ooids (GN76-1J, pore 3). (B) Chalcedony in typical pore between peloids; first generation of cement is parallel-fibrous chalcedony isopachously coating clasts from numerous nucleation sites; second generation of cement is radial-fibrous (or botryoidal) chalcedony filling the center of pore by diverging from a much more restricted number of nucleation sites (GN76-7B, pore 2).

Chalcedony consists of fibrous crystals of quartz that grow relatively rapidly in one dimension to form either radial or parallel aggregates. Like druses, fibrous crystals compete with one another as they fill pores producing distinctive textures (Fig. 2B). Fibrous textures have been given various names including isopachous and botryoidal. Many chalcedonic cements in GIFs have experienced fine-scale recrystallization involving crystal boundary migration while retaining most of their optical orientation. As the optical orientation becomes progressively more random, these pass into a texture Simonson (1987) referred to as "domain cement." We included one sample with chalcedonic cement that did not show any textures indicative of recrystallization for analysis (see Section 4 for details).

Samples displaying evidence of significant compaction prior to cementation are more likely to have remained open to pore water exchange at greater depth and therefore are less likely to be informative about seawater chemistry. Textural characteristics indicative of compaction include a high number of contacts per grain and the deformation of clasts by either physical processes or pressure solution. Such textures are common in GIFs (e.g., Simonson, 1987, Figs. 2C, 3C, and 4A, D) and even appear locally in samples that have a high minus-cement porosity elsewhere. In order to obtain the earliest geochemical signal possible, we avoided analyzing samples and areas that displayed overt evidence of compaction in selecting our spots for ion microprobe analysis.

3. Analytical methods

3.1. Cathodoluminescence

Cathodoluminescence (CL) images were collected using the Cameca SX 100 electron probe microanalyzer at University of Michigan with an accelerating voltage of 15 kV and a beam current of 40 nA. Using a transmitted light microscope, cross-polarized images corresponding to the exact area of each CL image were collected for reference. These images were then superimposed on the CL image for comparison of crystal boundaries with CL zones and selection of ion microprobe analysis pits (see Figures in Supplementary Materials for examples).

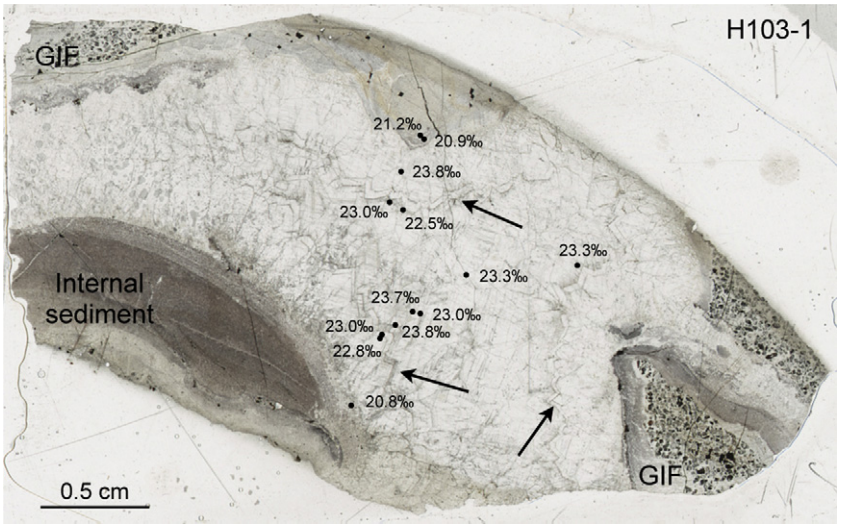

Fig. 3. Photograph (plane-polarized light) of an entire large-format thin section with a large vug in a Sokoman GIF (H103-1). The host sediment is visible along edges in lower right and upper left where peloids and cement are both sharply truncated and coated with a band of fine hematitic chert (light gray). After a thicker, geopetal accumulation of mostly darker internal sediment was deposited, coarsely crystalline quartz cement (clear) filled the rest of the vug. The quartz crystals contain veils that are roughly concentric to the edges of the vug and indicate the crystals grew centripetally inwards from all edges. The arrows point to a distinctive pair of closely spaced veils present in crystals growing inward from three different sides of the vug. $\delta^{18}O$ values are in ‰ VSMOW.

3.2. Oxygen isotope analyses

Five thin sections were selected for ion microprobe analysis after CL imaging. Standard thin sections were ground into 25.4 mm round sections, then crystals of University of Wisconsin quartz standard (UWQ-1, $\delta^{18}O = 12.33 \pm 0.07$‰ VSMOW; Kelly et al., 2007) were embedded in the centers of the thin sections and polished to be co-planar with the sample. Prior to analysis, samples were cleaned and coated with carbon.

Oxygen isotope analyses were performed using the WiscSIMS Cameca ims1280 ion microprobe at the University of Wisconsin-Madison using the methods described in Kita et al. (2009) and Valley and Kita (2009). The primary $^{133}Cs^{+}$ ion beam was focused to 10 μm × 15 μm at 2 nA and secondary O^{-} ions were detected using multi-collection Faraday cups with typical ^{16}O intensity of 2.5×10^{9} cps. All measurements on the five samples were collected in one analytical session over the course of 12 h on January 29, 2009. At least four standard analyses before and after each group of ten, or fewer, sample analyses were used to correct the data. The average of these eight bracketing standard analyses determined the instrumental bias based on the accepted UWQ-1 value of 12.33‰ (Kelly et al., 2007). External errors based on the reproducibility of UWQ-1 ranged from 0.29 to 0.41‰ (±2SD, spot-to-spot).

After ion microprobe analysis, samples were examined on a scanning electron microscope (SEM) at Oberlin College. Pit shapes were classified using the terminology of Cavosie et al. (2005). Data from six irregular pits that were located on cracks or contained inclusions were excluded, but are presented for completeness in Supplementary Materials Table A. Inclusion of irregular pits would shift sample averages by less than 0.2‰.

4. Petrography

4.1. Transmitted light

We analyzed 5 samples of GIFs with high minus-cement porosities (Table 1), three from the Gunflint Iron Formation and two from the Sokoman Iron Formation. As described in Section 2.3, the framework clasts in all 5 samples are sand-sized (0.63–2 mm) peloids and ooids that consist largely of chert, iron silicate (mainly greenalite), and/or hematite. The sizes of the intergranular pores range from 0.2 to 1 mm across. Some of the GIF samples also contain unusually large pores that would have been strongly compacted if they had not been buttressed with cement before significant burial. Both the intergranular and larger pores we studied are filled with drusy to blocky quartz and/or chalcedony interpreted as primary cements. The specific characteristics of the samples are described below.

Sample GN76-7B is from the Gunflint Iron Formation. Its clasts are almost all uniform, medium/coarse sand-size, chert–hematite peloids, a few of which contain some fine iron silicates. The sample contains 69% clasts and 31% chalcedonic cement by volume and was collected from the center of a well-cemented pod that we interpret as an early diagenetic concretion. Along the edges of this pod, the peloids are largely converted to greenalite whereas most of the chalcedonic cement has been replaced by coarsely crystalline carbonate that locally pseudomorphs the growth bands of the chalcedony. While the sample we analyzed is from the center of the pod, locally it contains large carbonate euhedra that replace both clasts and cement.

Sample GN76-8 from the Gunflint Iron Formation consists largely of greenalite–chert peloids in the medium to coarse sand size range, some of which have thin oolitic rims. The sample also contains a scattering of tabular greenalite intraclasts up to 5 mm long. Clasts make up 80% of the sample and drusy intergranular cement makes up the other 20% by volume.

Sample GN76-1J, also from the Gunflint Iron Formation, is the most diverse. The GIF in this sample consists largely of ooids of greenalite-rich chert and some hematite that range in size from fine to very coarse sand. Also present are some tabular intraclasts of BIF-like silicate up to 2 cm long beneath which are large vugs in the form of shelter porosity. Locally the sediment is replaced by coarsely crystalline carbonate and displays acicular sprays of hematitic crystals of an unknown origin. All of this sediment is adjacent to a columnar chert stromatolite. In areas with high-minus cement porosity, the intergranular and shelter pores are filled with drusy quartz. In other areas, the intergranular quartz forms an equigranular polygonal network, but we analyzed only areas displaying void-filling textures.

Sample HR77-5A is from the Sokoman Iron Formation in the Howells River area where stromatolites are unusually abundant (Klein and Fink, 1976). The sample includes part of a domal stromatolite core with GIF that consists of medium sand-size greenalite peloids. The GIF also contains tabular cherty intraclasts up to 6 mm long that appear to be intraclasts eroded from similar stromatolites. Clasts make up roughly 66% and silica cements the remaining 34% by volume of this GIF. The high minus-cement porosity, the lack of compaction features, and the fact that it is directly coated by stromatolitic laminations all indicate this GIF was cemented very early. However, the quartz in the cements is more equidimensional, i.e., blocky, and less elongated than crystals in classic druses; this suggests the cements in this particular sample may have undergone some recrystallization. In addition, it is locally replaced by euhedral magnetite crystals that replaced both clasts and cement.

Sample H103-1 from the Sokoman Iron Formation is texturally quite different from the other samples. It contains a large filled-in vug in a GIF comprised of well-sorted, medium sand-sized hematite–chert peloids (Fig. 3). Although this GIF has high minus-cement porosity, its intergranular cement appears to be neomorphosed and/or recrystallized as it displays domain texture. The peloids also appear more neomorphosed than in other samples as most consist of mosaics of equidimensional quartz crystals that are larger than those in other samples. The vug likely formed via syneresis in the already cemented GIF prior to neomorphism. Along the presumed bottom of the vug is internal

Table 1
Locations and summary of petrographic features of analyzed samples.

Sample	Location		Clasts		Cement textures		Miscellaneous other features		
	Latitude	Longitude	Peloids	Ooids	Druse	Chalcedony	Vugs	Stromatolite	Internal sediment
Gunflint									
GN76-1J	48°17.1′N	89°50.5′W	–	x	x	–	x	x	–
GN76-7B	48°25.2′N	89°15.9′W	x	–	Trace	x	–	–	–
GN76-8	48°25.8′N	89°15.5′W	x	Trace	x	–	–	–	–
Sokoman									
H103-1	54°51.5′N	67°1.8′W	x	–	x[a]	–	x	–	x
HR77-5A	54°54.1′N	67°15.2′W	x	–	x[b]	–	–	x	–

[a] Refers to cement filling vug, not intergranular pores.
[b] Cement is more blocky than those in other drusy samples.

sediment approximately 1 cm thick consisting of fine hematitic chert overlain by coarser sediment showing some low-angle cross-stratification (Simonson, 1987, Fig. 8B); this indicates the vug was open to the sediment–water interface at the time the internal sediment was emplaced. Drusy quartz crystals up to 6 mm long with well-developed veils subsequently nucleated on top of this internal sediment (Fig. 3).

4.2. Cathodoluminescence

Eleven pores from the five samples were imaged by CL and a variety of subtle, but unmistakable zoning patterns emerged. These patterns can be divided into four main categories based on the appearance of CL domains caused by variations in intensity:

(i) Chevrons close to the edges of pores defined by narrow, low intensity or dark CL bands (Fig. 4A). The chevron pattern is best seen in narrow, dark bands of lower CL intensity that outline peaks and reentrants in CL zones; they are visible to some degree in all samples showing variable CL intensity, usually near pore edges. Based on CL images superimposed over cross-polarized images of the same pore at the same scale, the reentrants in zones defined by changes in CL intensity clearly coincide with boundaries between adjacent quartz crystals (Figs. A–D, Supplementary Materials). This relation is clearest between chevron-type CL bands and cement crystals close to clast edges (Fig. 4A).
(ii) Wider, low-intensity dark-CL bands still mimicking the shapes of pores but with a more blocky polygonal pattern (Fig. 4B). Zones with lower intensity luminescence in the blocky patterns are similar to, but thicker than, the zones in the best defined chevrons. Blocky patterns are most distinct in sample HR77-5A.
(iii) Mottled patterns without clearly defined CL bands concentric to the pore edges (Fig. 4D). Mottled CL is common in the centers of pores, particularly larger pores where 3D effects are more pronounced. Sample GN76-8 has the greatest number of pores with mottled CL. Instead of concentric bands, variations in CL intensity in these mottled pores are complex near pore edges, with larger zones of a particular CL intensity appearing in the middle of the pore.
(iv) Pores that show little variation in CL intensity. In our initial examination, we found at least one pore showing pattern iv, i.e., no obvious variation in CL intensity, in three of five samples. We had hoped to see dramatic contrasts in CL intensity in the druse crystals parallel to the veils in sample H103-1 (Fig. 3), but the CL turned out to be uniform in intensity in these crystals.

Patterns defined by changes in CL intensity, e.g., from dark to bright across a pore, are consistent between pores displaying the same category of zoning within a given sample. However, pores within a sample can display a different number of bands depending on which zoning patterns are present. Combinations of different types of zoning patterns are noticeable within pores in some cases. For example, mottled pores may appear to have an ill-defined band of chevrons near the edges of the clasts surrounding the pore. Similarly, sample HR77-5A contains a pore with blocky zonation plus a band of chevrons along one edge (Fig. B, Supplementary Materials). The sample with chalcedonic cement is most consistent in terms of the variation of the intensity of the luminescence from pore to pore. In contrast to both the chevron and blocky patterns seen in the other samples, the bands in the chalcedonic cement conform to the hemispheric patterns typical of radial-fibrous or botryoidal growth patterns (Fig. 4C). In these botryoidal growth areas, the intensity of the luminescence is low near the peloids and high in the center of all three pores examined. For our later $\delta^{18}O$ analyses, we strived to sample from each CL zone apparent in a given pore.

5. Oxygen isotopes

Isotope analyses were guided by our observations of CL zoning. Within the eleven pores imaged by CL, a total of 54 $\delta^{18}O$ analyses (40 in pore-filling cements and 14 within clasts) are presented below. With one exception, all pits in clasts are from the Gunflint, as most pure-quartz patches in clasts from the Sokoman samples were too small for analysis or yielded irregular pits. Raw and corrected data for all samples and standards is presented in Table A, Supplementary Materials.

The $\delta^{18}O$ of quartz cements from Gunflint samples ranges from 23.5 to 26.4‰ VSMOW, with an average of 24.4‰ (Table 2). The earliest-formed cements in the vug sample from the Sokoman Iron Formation (H103-1) have similarly high $\delta^{18}O$ values (23.8‰) but range to lower $\delta^{18}O$ in the later-formed quartz in the center of the vug (20.8‰). The Sokoman sample with possibly neomorphosed cements (HR77-5A) records substantially lower $\delta^{18}O$ (18.9–19.4‰) than other samples. Clear quartz patches within Gunflint clasts are likely neomorphosed, but still range from 21.3 to 26.8‰, averaging 24.1‰.

Significant variation (beyond analytical uncertainty) between at least two pits is present in some pores (e.g., Figs. 4A and C). However, typical variability in the cement within a given pore is on the order of 0.4‰, at the limit of analytical uncertainty. The greatest variation observed is across a single vug-filling veiled crystal 6 mm long within Sokomon sample H103-1 (Fig. 3). Three analyses made closest to the internal sediment (Fig. 3, pits G, L, K) have values ~2‰ lower than 10 pits that are more centrally located and presumably formed later. However, the isotopic values of cement in a single pore in sample GN76-7B show the opposite pattern (Fig. 4C): the most centrally located one (pit I, 23.9‰) has a lower $\delta^{18}O$ than those located nearest the peloids, which presumably formed earlier (pit E, 25.2‰). In sample GN76-1J, there are differences of up to 2.7‰ between pits that are both centrally located in pores (Fig. 4A, pits C and F). Two pits in the same CL band have values that differ by 2.0‰ (Fig. 4A, pits C and D). Three pits analyzed in a second, smaller pore of sample GN76-1J show no variation in $\delta^{18}O$. Neither HR77-5A nor GN76-8 show any significant variation in $\delta^{18}O$ between the center and edge of the one pore with multiple pits in both areas of each sample.

Quartz within Gunflint clasts has $\delta^{18}O$ values that are significantly different than the pores (Fig. 5). In two samples, GN76-1J and GN6-7B (Fig. 4A and C, respectively), the quartz in the clasts has lower $\delta^{18}O$ than the quartz cement in adjacent pores. However, in sample GN76-8 (Fig. 4D), clast values are higher than cement values. This contrast is not a function of any regional variation because GN76-7B and GN76-8 were collected in relatively close proximity to one another whereas GN76-1J was collected ~45 km away to

Table 2
Summary of oxygen isotope analyses by ion microprobe (‰ VSMOW) of silica from Gunflint and Sokoman GIFs.

Sample	$\delta^{18}O$ of silica cements		$\delta^{18}O$ of clasts
	Range	Average	Range
GN76-1J	23.5–26.4	24.4	21.3–25.0
GN76-7B	23.7–25.1	24.4	22.9–23.1[a]
GN76-8	24.3–24.9	24.6	25.1–26.8
H103-1	20.8–23.8	22.6	nd
HR77-5A	18.9–19.4	19.2	19.5[b]

nd = not determined.
[a] Only two peloid values for this sample.
[b] Only one peloid value for this sample.

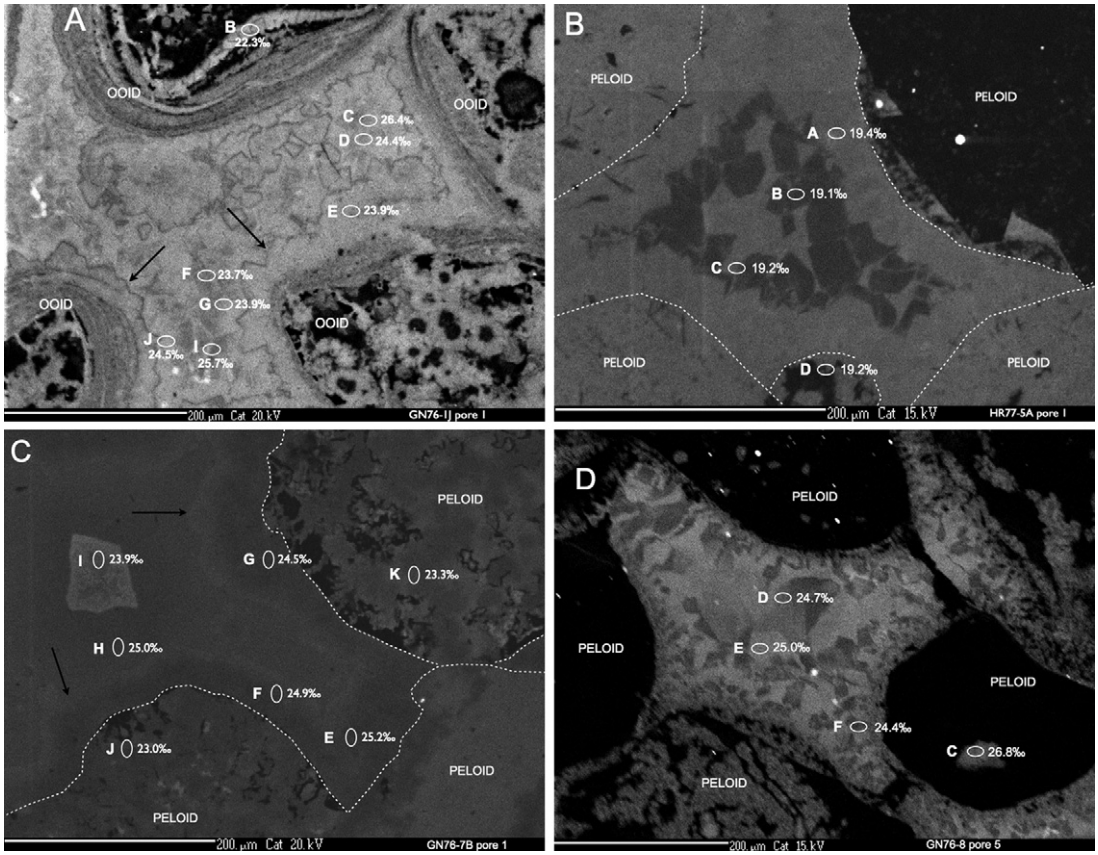

Fig. 4. Cathodoluminescence images of cements from GIFs. Where they are not obvious, clast edges are indicated by dashed lines. The locations of ion microprobe analysis points are indicated by white ellipses with $\delta^{18}O$ indicated in ‰ VSMOW. (A) Sample GN76-1J, pore 1. One narrow dark band (arrows) gives definition to chevrons roughly concentric to pore edges; polygonal zoning in the middle of the pore is likely zoned quartz crystals growing into the plane of the thin section from above or below. Curving light band inside ooid along upper edge (with pit B in it) is probably quartz cement filling a syneresis crack. Uncertainty is ±0.4‰ (2 SD). (B) Sample HR77-5A, pore 2. Thicker dark band gives definition to chevrons that are similar to those in A but more blocky in appearance; uncertainty is ±0.4‰. (C) Sample GN76-7B, pore 2. Chalcedonic cements with faint banding (arrows) roughly concentric to pore edges outlining botryoidal growth zones; brightest zone is in the pore center; uncertainty is ±0.5‰ (D) Sample GN76-8, pore 3. Cement with mottled CL pattern; the tendency for crystals to increase in size towards pore centers typical of druse is evident, but CL bands concentric to pore edges are not; uncertainty is ±0.3‰.

the west (Table 1). A complicating factor is the possible presence of cements inside clasts. Although the bulk of the quartz in the clasts must have formed via neomorphism of poorly ordered precursors, shrinkage cracks that probably formed via syneresis are present in many clasts (e.g., Fig. 4A) and cements may have filled them in addition to the intergranular pores.

6. Discussion

6.1. Optical and CL petrography

Sedimentary textures apparent in the samples (described in Sections 2.3 and 4.1) suggest at least initial cementation of the GIFs we studied took place very close to the sediment–water interface. Evidence for this conclusion includes the high minus-cement porosity of the GIFs (Fig. 1A), the presence of well-rounded GIF intraclasts in high-energy layers in both Gunflint and Sokoman Iron Formations (Fig. 1B), the local presence of internal sediment in some of the larger voids (Fig. 3), and the growth of some stromatolites on a substrate of GIF. Both the occurrence of rip-up clasts consisting of well-sorted sand grains and internal sediment in cracks and vugs that cut across clasts and cements require cementation very close to the sediment–water interface. The presence of cross-laminated internal sediment within the large vug in H103-1 provides particularly persuasive evidence that, at least for a while, the waters in this pore were in communication with the seawater above. While the large vugs in GN76-1J do not contain any internal sediment, their survival with no perceptible compaction again suggests little burial occurred prior to the onset of cementation. Finally, the construction of a stromatolite on GIF as in sample HR77-5A requires induration of a well-sorted sand at the sediment–water interface. Either the GIF was eroded and subsequently coated by stromatolitic laminations in situ (essentially forming a hardground) or it represents a pebble- to cobble-size intraclast of cemented GIF on which a stromatolite grew after it came to rest; either way, the GIF on which the stromatolite grew, whose cement consists entirely of silica, was cemented at or very close to the sediment–water interface.

Regardless of how early they formed, the drusy and chalcedonic textures present in many of the pore fillings of our samples signify that these are primary void-filling quartz cements rather than amorphous precipitates that were neomorphosed later in diagenesis. The preservation of different zones of CL intensity across pore-filling cements suggests that the crystals preserve compositional heterogeneity formed during initial growth. Common causes of luminescence include point defects, dislocations and microinclusions (Marshall, 1988; Götze, 2009). Foreign ions in the quartz lattice can activate (e.g., Al, Mn, Ti) or quench (e.g., Fe) CL emission (Sippel, 1968; Marshall, 1988). Authigenic quartz typically has weaker luminescence than detrital quartz because few activator ions are incorporated during low-temperature growth processes (Sippel, 1968; Marshall, 1988). Trace element variations of one order of magnitude have been found across zoned quartz crystals; this variation, apparent in CL images, is most likely due to changes

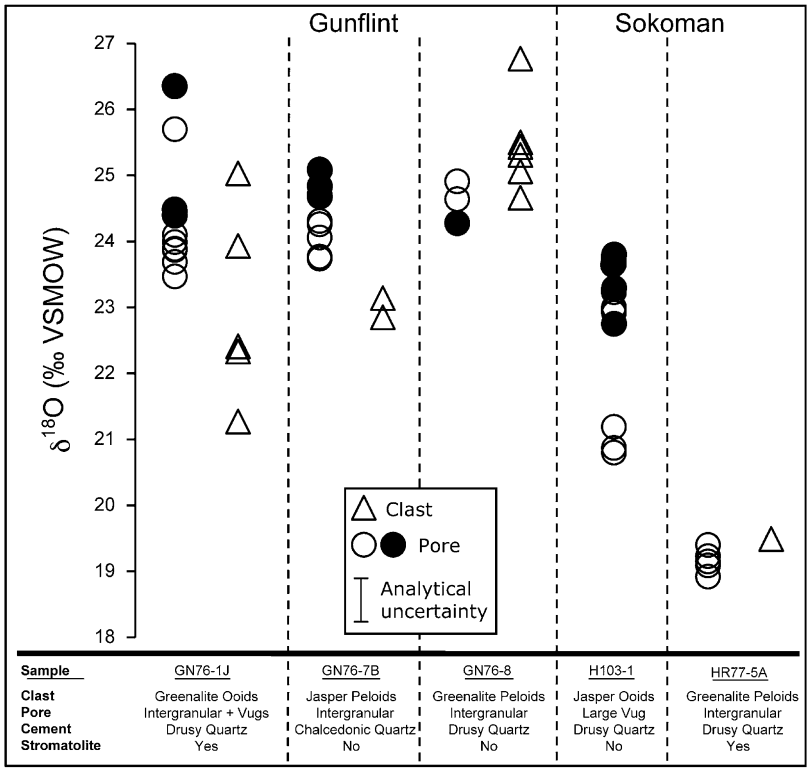

Fig. 5. Summary of ion microprobe $\delta^{18}O$ analyses of quartz cements (circles) compared with framework clasts (triangles) in samples from the Gunflint and Sokoman Iron Formations. Filled circles indicate texturally earliest cement analyses (i.e., pits close to clast edges) whereas open circles indicate later cements (i.e., pits closer to pore centers). Uncertainty of analyses is 0.4‰ (2 SD). Petrographic features of the samples are summarized at bottom.

in fluid composition rather than other factors such as temperature variation or growth speed (Perny et al., 1992). The existence of variation in the CL of quartz cements in these iron formations suggests a changing fluid environment during cementation.

CL patterns and veils show similar chevron-style geometries expected from void-filling cements. Although sample H103-1 is characterized by CL that is uniform in intensity, the presence of veils in transmitted light provides similar textural information. Uniform CL intensity does not eliminate the possibility that a single crystal has grown under variable conditions over a long time span. For example, Sippel (1968) found a lack of CL contrast between some detrital cores and their cement overgrowths, clearly showing that quartz crystals with different zones grown under very different conditions can have the same CL intensity.

Based on our observations, pores smaller than 0.05 mm^2 are more likely to consistently show distinct banding that is easily interpreted as growth zoning (Fig. 4A), while larger pores are more likely to have a mottled appearance or luminescence with constant intensity (Fig. 4D). A mottled effect may be a result of larger pores having a higher incidence of oblique cuts through crystals growing perpendicular to the plane of the thin section. As a consequence, the plane of the thin section crosses through more zones at a shallow angle, changing the apparent thickness of the zones. This effect can be recognized in conventional microscopy as polyhedral extinction as opposed to extinction of a single crystal. Alternatively, complex luminescence patterns, which may include mottled pores such as we saw, can result from distorted growth in regions of rapid crystal formation (Perny et al., 1992). Then again, rapid crystal growth could result in more uniform CL in part because there is simply less time for the geochemistry of the precipitating fluid to change.

Superposition of CL images from this study over corresponding crossed-polarized optical images allowed observation of relations between CL zones and optical extinction units in individual pores (Figs. A–D, Supplementary Materials). Comparison is complicated by the fact that the CL images are strictly two-dimensional, whereas extinction behavior involves a third (albeit narrow) dimension. Nevertheless, reentrants in growth zones defined by variations in the intensity of the luminescence coincide with crystal boundaries determined optically. Embayments in CL chevrons match contacts between crystal pairs. Such correlation supports the inference that the pore-filling textures in the crystals are not neomorphosed or recrystallized, processes that could homogenize crystal composition. This in turn serves as an additional line of evidence that the pore-filling cements are primary.

Even chalcedonic cements, characterized by higher surface area to volume ratios than drusy crystals, preserve CL growth bands that are concentric to the nucleation points of radial-fibrous fans and continuous from fan to fan (Fig. 4C); this is consistent with radial-fibrous growth. In the chalcedonic sample, CL bands correspond to the growth progression from an isopachous rim around the peloids to radial aggregates of pore-filling fibers. The botryoidal arcs formed by radial aggregates are evidenced in the CL images by the rounded reentrants in CL zones. The preservation of CL variation across chalcedony fibers is further evidence that these cements are unrecrystallized.

6.2. Oxygen isotopes

Petrographic and CL observations confirm that most of the analyzed cements are unneomorphosed, void-filling, and early-forming. This suggests that the $\delta^{18}O$ observed in these cements is preserved from the time of quartz growth, barring modification by diffusion. The essentially unmetamorphosed nature of the Gunflint and Sokoman samples makes it unlikely that intragranular diffusion is responsible for the isotopic compositions measured. The similarity in $\delta^{18}O$ of quartz in clasts, surrounded by lower $\delta^{18}O$ minerals

and the $\delta^{18}O$ of quartz at the margin of pores within ~20 μm clasts (e.g., Fig. 4) with that of quartz in the center of pores, precludes any substantial resetting.

Fibrous chalcedonic cements are more likely than drusy quartz cements to lose their primary isotopic composition to diffusion due to their much higher surface area to volume ratio. Yet, the chalcedony in sample GN76-7B (Fig. 4C) retains primary growth zoning in both CL and $\delta^{18}O$, further evidence against homogenization by diffusion or any other process. Some additional degree of uncertainty must be added to $\delta^{18}O$ analyses of chalcedony by ion microprobe which is normalized using a coarsely crystalline quartz standard, and any difference in instrumental bias between chalcedony and quartz is not tightly constrained. However, samples of opaline silica, measured at WiscSIMS, have the same instrumental bias as the UWQ-1 quartz standard, but because the opal is heterogeneous at the ±1‰ level, this is not yet a precise determination (T. Ushikubo, personal communication). Furthermore, the isotopic values for the chalcedonic cement are similar to quartz cements in other Gunflint samples (Fig. 5), and the tight range of $\delta^{18}O$ preserved in all the samples in this study suggests that any additional analytical uncertainty is minor.

Our preferred interpretation of data for Gunflint samples is that the real, but limited variability of $\delta^{18}O$ observed reflects small local temperature and/or compositional variability of pore waters. The isotopic variability further supports the interpretation of the CL patterns observed in the cements (Fig. 4) as growth banding in primary quartz crystals, and the limited variability would be consistent with open-system pore fluids.

Samples from the Sokoman Iron Formation require modifications to this model to explain the textural and isotopic variability observed. In particular, sample HR77-5A, although texturally similar to the Gunflint GIFs, has a substantially lower $\delta^{18}O$ (18.9–19.4‰). If the $\delta^{18}O$ is primary, the low values are inconsistent with the other samples and any reasonable ocean temperature, and so must be the result of precipitation from fluids at a higher temperature or a lower $\delta^{18}O$. Hydrothermal vein quartz analyzed by Marin et al. (2010) from the Gunflint has an average $\delta^{18}O$ of 19.4‰, similar to cements in HR77-5A. Quartz cements are more blocky in this sample than in other GIFs, suggesting they were recrystallized. However, cement recrystallization with a concomitant change in $\delta^{18}O$ in this sample is difficult to reconcile with the apparently undisturbed CL zoning. Additional study of CL in iron formation sediments is clearly required to better understand these results. The second Sokoman sample (H103-1) contains a large vug with $\delta^{18}O$ values varying from edge to center by up to 2‰. But, the high $\delta^{18}O$ of quartz in the earliest-formed cements close to pore margins are consistent with what is observed from the Gunflint Iron Formation.

Unrecrystallized quartz cements from GIFs appear to preserve primary $\delta^{18}O$ formed in equilibrium with pore waters, but the relationship between those pore waters and seawater must be evaluated. Pore waters found at significant depth would have higher temperatures than seawater due to the geothermal gradient and therefore form quartz cements with lower $\delta^{18}O$ than would be formed directly in equilibrium with the overlying ocean, consistent with what we observe in central portions of pores in sample GN76-7B (Fig. 4C). Furthermore, deep pore waters may become isolated from larger reservoirs, and may have $\delta^{18}O$ substantially fractionated by reaction with quartz in a quasi-closed system, such as the later-forming central portion of the vug sample (H103-1, Fig. 3). However, petrographic evidence presented above suggests the portions of the intergranular cements closest to clast margins began forming close to the sediment–water interface. The water that was in equilibrium with these earliest-formed cements cannot plausibly have been substantially warmer nor had a very different $\delta^{18}O$ than the sea only meters above. The fact that the variability in $\delta^{18}O$

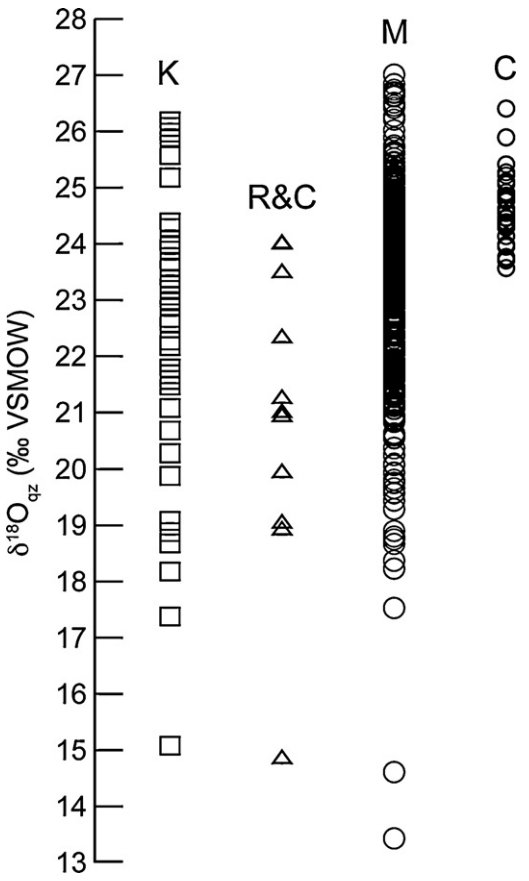

Fig. 6. Comparison of quartz $\delta^{18}O$ analyses of the Gunflint Iron Formation by different researchers. K = Knauth (2005, fluorine extraction); R&C = Robert and Chaussidon (2006, ion microprobe); M = Marin et al. (2010, ion microprobe); and C = this study.

recorded as the cements filled pore space is only about 1–2‰ is similarly consistent with only minor changes in temperature and isotopic composition as these sediments were buried. Although we have no modern analogue for GIF formation, direct analysis of well-flushed modern pore waters in carbonates indicates that $\delta^{18}O$ values vary only on the order of 1–2‰ within the first 100 meters of sediment below the sea floor (Schrag et al., 1996; Hesse et al., 2000; Swart, 2000; Adkins and Schrag, 2001), consistent with our observations.

The isotopic values presented in this study are the result of in situ microanalysis guided by petrographic identification of samples with well preserved, demonstrably unrecrystallized cements that formed in equilibrium with waters close to the sea floor. The $\delta^{18}O$ of unneomorphosed cements from the Gunflint Iron Formation (23.5–26.4‰) are similar to the highest values previously reported for recrystallized silica from the Gunflint Iron Formation (Fig. 6) either measured by fluorine extraction (Winter and Knauth, 1992a; Knauth, 2005) or by ion microprobe (Robert and Chaussidon, 2006; Marin et al., 2010). However, the data presented here has substantially less scatter in $\delta^{18}O$. Based on a correlation between silicon and oxygen isotopes, Robert and Chaussidon (2006) suggested that only cherts with $\delta^{18}O$ within 6‰ of the highest measured value for a given locale were likely to preserve primary values. That range is substantially larger than the 3.1‰ range in unneomorphosed cements presented here.

Marin et al. (2010) analyzed quartz in a variety of textures from the Gunflint Iron Formation by ion microprobe, focusing primarily on the microquartz formed by neomorphism of the amorphous silica precursor. Their data on microquartz are highly variable, and they interpret this as a result of diagenetic processes. By modeling

the highly variable $\delta^{18}O$ of microquartz, these workers arrived at slightly higher $\delta^{18}O$ silica precursor for microquartz (27‰), similar to the highest values for cements measured directly in this study. The similarity of quartz isotopic composition among these studies and the present work suggests that the highest $\delta^{18}O$ preserved in conventionally analyzed cherts is at least close to the primary value.

Translating a primary $\delta^{18}O$ record in quartz into water temperatures is not straightforward, however. Estimates of water temperature require knowledge of not only the $\delta^{18}O$ of primary quartz, but also the $\delta^{18}O$ of the water in equilibrium with the quartz and a calibration of the equilibrium fractionation. Application of the Knauth and Epstein (1976) thermometer using an estimated $\delta^{18}O_{SW} = -1‰$ as applied by previous workers on the Gunflint Iron Formation yields temperatures of ~45–60 °C from early-formed cements, similar to those of previous workers (e.g., Winter and Knauth, 1992a; Marin et al., 2010). Significant uncertainty remains in both the composition of water, and the calibration of the thermometer. There are many calibrations of the quartz–water fractionation available based on different theoretical and experimental methods, which yield broadly similar results (e.g., Clayton et al., 1972; Bottinga and Javoy, 1973; Kawabe, 1978; Matsuhisa et al., 1979; Ligang et al., 1989) but which also impose an uncertainty of ~15° on any temperature calculation. Furthermore, even if secular evolution of seawater is within 3‰ of the modern ice-free value, that translates into an additional uncertainty in temperature of ~15 °C. Improved calibrations of the quartz–water thermometer and a better understanding of secular change in seawater $\delta^{18}O$ are greatly needed to reduce this considerable uncertainty.

Just as all waters sampled from modern seas are not necessarily representative of global ocean composition and temperature, we should not expect all seawater to be the same at any point in the Precambrian. In light of the fact that the high-energy processes needed to produce GIFs are only found in shallow environments, our results may be biased towards water temperatures that are warmer than the global mean of the ocean. The composition of seawater is also more likely to depart from the global mean in shallow-water environments. It has been suggested that the Sokomon Formation formed at low latitudes, namely 3–5° (Williams and Schmidt, 2004). This would compound the problem as shallow waters at low latitudes would presumably have some of the highest temperatures to be found anywhere in the global ocean. Furthermore, the Gunflint Iron Formation may have formed in a relatively restricted basin, characterized by stratified waters and substantial fresh water input (Pufahl et al., 2010). The presence of a meteoric water component could also contribute to lower $\delta^{18}O$ values than those found in the open ocean today. An ejecta layer from the Sudbury impact was deposited at 1.85 Ga as the deposition of the Gunflint Iron Formation was ending; studies of this layer and associated strata suggest the area around Thunder Bay may have been subaerially exposed for some time (Addison et al., 2010). However, any meteoric circulation through these strata could not have persisted for too long because both the Gunflint and Sokoman Iron Formations are overlain by thick shale-turbidite successions deposited in deep marine paleoenvironments (Simonson, 1985).

7. Concluding thoughts

Sedimentary petrographic scrutiny prior to in situ oxygen isotope analysis allowed us to say with a measure of certainty that the quartz cements we analyzed are formed early in diagenesis and some consist of quartz crystals that are clearly primary, i.e., unrecrystallized since precipitation. Variability in $\delta^{18}O$ across single pores as well as individual cement crystals strongly suggests our values reflect original isotopic compositions of, and limited fluctuations in, pore water conditions close to the Precambrian seafloor in a high-energy shallow shelf environment. However, converting these measurements into global sea temperatures and compositions remains problematic. In our pilot study, we attempted to assess the possibility of identifying primary to early diagenetic phases petrographically (see also, Winter and Knauth, 1992b) in order to analyze them by in situ geochemical methods. We believe our preliminary results suggest that such an approach is feasible. The quartz crystals analyzed yield $\delta^{18}O$ that was substantially lower than modern cherts, consistent with a large body of previous work on Precambrian cherts (Knauth, 2005; Marin et al., 2010; Marin-Carbonne et al., 2011; and references therein). However, the waters of iron formation basins may not have been in open connection with the world ocean (Pufahl et al., 2010), and more work is required to characterize and understand this important secular change.

Acknowledgements

Petrographic research was supported by grants from Oberlin College and NASA (NNX08AI29G). Thanks are extended to Eric Essene and Carl Henderson at the University of Michigan for access to and assistance with the electron probe microanalyzer used to obtain CL images. We also thank Hubert Bates and Peter Munk for preparing the thin sections, Noriko Kita for assistance with ion microprobe analysis, and Andrey Bekker and 2 anonymous reviewers for valuable feedback on our initial draft. Geochemical research was partly supported by the NASA Astrobiology Institute, DOE (93ER14389), and Oberlin College. The acquisition of the SEM at Oberlin College used in this study was supported by NSF-CCLI (0087895). WiscSIMS is partly supported by NSF-EAR (0319230, 0744079, 1053466).

Appendix A. Supplementary data

Supplementary data associated with this article can be found, in the online version, at doi:10.1016/j.precamres.2012.01.016.

References

Addison, W.D., Brumpton, G.R., Davis, D.W., Fralick, P.W., Kissin, S.A., 2010. Debrisites from the Sudbury impact event in Ontario, north of Lake Superior, and a new age constraint: Are they base-surge deposits or tsunami deposits? In: Gibson, R.L., Reimold, W.U. (Eds.), Large Meteorite Impacts and Planetary Evolution IV, vol. 465. Geological Society of America Special Paper, pp. 245–268.

Adkins, J.F., Schrag, D.P., 2001. Pore fluid constraints on deep ocean temperature and salinity during the last glacial maximum. Geophys. Res. Lett. 28, 771–774.

Awramik, S.M., Barghoorn, E.S., 1977. The Gunflint microbiota. Precambrian Res. 5, 121–142.

Beard, D.C., Weyl, P.K., 1973. Influence of texture on porosity and permeability of unconsolidated sand. Am. Assoc. Petrol. Geol. Bull. 57, 349–369.

Bekker, A., Slack, J., Planavsky, N., Krapez, B., Hofmann, A., Konhauser, K.O., Rouxel, O.J., 2010. Iron formation: the sedimentary product of a complex interplay among mantle, tectonic, oceanic, and biospheric processes. Econ. Geol. 105, 467–508.

Beukes, N.J., Gutzmer, J., 2008. Origin and paleoenvironmental significance of major iron formations at the Archean–Paleoproterozoic boundary. In: Hagemann, S., Rosiere, C., Gutzmer, J., Beukes, N.J. (Eds.), Banded Iron Formation-Related High-Grade Iron Ore, vol. 15. Society of Economic Geology Reviews in Economic Geology, pp. 5–47.

Bottinga, Y., Javoy, M., 1973. Comments on oxygen isotope geothermometry. Earth Planet. Sci. Lett. 20, 250–265.

Cavosie, A.J., Valley, J.W., Wilde, S.A., EIMF, 2005. Magmatic $\delta^{18}O$ in 4400–3900 ma detrital zircons: a record of the alteration and recycling of crust in the early Archean. Earth Planet. Sci. Lett. 235, 663–681.

Clayton, R.N., O'Neil, J.R., Mayeda, T.K., 1972. Oxygen isotope exchange between quartz and water. J. Geophys. Res. 77, 3057–3067.

Cole, D.R., Chakraborty, S., 2001. Rates and mechanisms of isotopic exchange. In: Valley, J.W., Cole, D.R. (Eds.), Stable Isotope Geochemistry. Reviews in Mineral. & Geochem, vol. 43, pp. 83–224.

Dimroth, E., Chauvel, J.-J., 1973. Petrography of the Sokoman Iron Formation in part of the central Labrador trough. Geol. Soc. Am. Bull. 84, 111–134.

Enos, P., Sawatsky, L.H., 1981. Pore networks in Holocene carbonate sediments. J. Sed. Petrol. 51, 961–985.

Floran, R.J., Papike, J.J., 1975. Petrology of the low-grade rocks of the Gunflint Iron-Formation. Geol. Soc. Am. Bull. 86, 1169–1190.
Götze, J., 2009. Chemistry and physical properties of quartz – geological interpretation and technical application. Mineral. Mag. 73, 645–671.
Grigor'ev, D.P., 1965. Ontogeny of Minerals. Israel Program for Scientific Translations, Jerusalem, 250 pp.
Heck, P.R., Huberty, J.M., Kita, N.T., Ushikubo, T., Kozdon, R., Valley, J.W., 2011. SIMS analyses of silicon and oxygen isotope ratios for quartz in Archean and Paleoproterozoic banded iron formations. Geochim. Cosmochim. Acta 75, 5879–5891.
Hesse, R., Frape, S.K., Egeberg, P.K., Matsumoto, R., 2000. Stable isotope studies (Cl, O and H) of interstitial waters from site 998, Blake Ridge gas hydrate field, West Atlantic. In: Proc. Ocean Drilling Program Scientific Results, vol. 164, pp. 129–137.
Jones, D., Knauth, L., 1979. Oxygen isotopic and petrographic evidence relevant to the origin of the Arkansas novaculite. J. Sed. Petrol. 49, 581–598.
Karhu, J., Epstein, S., 1986. The implication of the oxygen isotope records in coexisting cherts and phosphates. Geochim. Cosmochim. Acta 50, 1745–1756.
Kawabe, I., 1978. Calculation of oxygen isotope fractionation in quartz–water system with special reference to the low temperature fractionation. Geochim. Cosmochim. Acta 42, 613–621.
Kelly, J.L., Fu, B., Kita, N.T., Valley, J.W., 2007. Optically continuous silcrete quartz cements of the St. Peter sandstone: high precision oxygen isotope analysis by ion microprobe. Geochim. Cosmochim. Acta 71, 3812–3832.
Kita, N.T., Ushikubo, T., Fu, B., Valley, J.W., 2009. High precision SIMS oxygen isotope analysis and the effect of sample topography. Chem. Geol. 264, 43–57.
Klein, C., 1978. Regional metamorphism of Proterozoic iron-formation, Labrador Trough, Canada. Am. Mineral. 63, 898–912.
Klein, C., 2005. Some Precambrian banded iron-formations (BIFs) from around the world: their age, geologic setting, mineralogy, metamorphism, geochemistry, and origin. Am. Mineral. 90, 1473–1499.
Klein, C., Fink, R.P., 1976. Petrology of the Sokoman Iron Formation in the Howells River area, at the western edge of the Labrador trough. Econ. Geol. 71, 453–487.
Knauth, L., 2005. Temperature and salinity history of the Precambrian ocean: implications for the course of microbial evolution. Palaeogeog. Palaeoclim. Palaeoecol. 219, 53–69.
Knauth, L.P., Epstein, S., 1976. Hydrogen and oxygen isotope ratios in nodular and bedded cherts. Geochim. Cosmochim. Acta 40, 1095–1108.
Knauth, L.P., Lowe, D.R., 1978. Oxygen isotope geochemistry of cherts from Onverwacht group (3.4 billion years), Transvaal, South Africa, with implications for secular variations in isotopic composition of cherts. Earth Planet. Sci. Lett. 41, 209–222.
Knauth, L.P., Lowe, D.R., 2003. High Archean climatic temperature inferred from oxygen isotope geochemistry of cherts in the 3.5 Ga Swaziland Supergroup, South Africa. Geol. Soc. Am. Bull. 115, 566–580.
Knoll, A.H., Simonson, B., 1981. Early Proterozoic micro-fossils and penecontemporaneous quartz cementation in the Sokoman Iron Formation, Canada. Science 211, 478–480.
Lee, M., Savin, S.M., 1985. Isolation of diagenetic overgrowths on quartz sand grains for oxygen isotopic analysis. Geochim. Cosmochim. Acta 49, 497–501.
Ligang, Z., Jingxiu, L., Huanbo, Z., Zhensheng, C., 1989. Oxygen isotope fractionation in the quartz–water–salt system. Econ. Geol. 84, 1643–1650.
Maliva, R.G., Knoll, A.H., Simonson, B.M., 2005. Secular change in the Precambrian silica cycle: insights from chert petrology. Geol. Soc. Am. Bull. 117, 835–845.
Marin, J., Chaussidon, M., Robert, F., 2010. Microscale oxygen isotope variations in 1.9 Ga Gunflint cherts: assessments of diagenesis effects and implications for oceanic paleotemperature reconstructions. Geochim. Cosmochim. Acta 74, 116–130.
Marin-Carbonne, J., Chaussidon, M., Boiron, M.-C., Robert, F., 2011. A combined in situ oxygen, silicon isotopic and fluid inclusion study of a chert sample from Onverwacht Group (3.35 Ga, South Africa): new constraints on fluid circulation. Chem. Geol. 286, 59–71.
Marshall, D.J., 1988. Cathodoluminescence of Geologic Materials. Unwin Hyman, Boston, 146 pp.
Matsuhisa, Y., Goldsmith, J.R., Clayton, R.N., 1979. Oxygen isotopic fractionation in the system quartz–albite–anorthite–water. Geochim. Cosmochim. Acta 43, 1131–1140.
Muehlenbachs, K., 2008. Revisiting the oxygen isotopic composition of the Archean ocean [abstract]. Geochim. Cosmochim. Acta 72, A659.
Muehlenbachs, K., Clayton, R.N., 1976. Oxygen isotope composition of the oceanic crust and its bearing on seawater. J. Geophys. Res. 81, 4365–4369.
Muehlenbachs, K., 1998. The oxygen isotopic composition of the oceans, sediments and the seafloor. Chem. Geol. 145, 263–273.
Perny, B., Eberhardt, P., Ramseyer, K., Mullis, J., Pankrath, R., 1992. Microdistribution of Al, Li, and Na in alpha-quartz: possible causes and correlation with short-lived cathodoluminescence. Am. Mineral. 77, 534–544.
Perry, E.C., Lefticariu, L., 2007. Formation and geochemistry of Precambrian chert. In: Mackenzie, F.T. (Ed.), Treatise on Geochemistry. In: Holland, H.D., Turekian, K.K. (Eds.), Sediments, Diagenesis, and Sedimentary Rocks, vol. 7, 2nd ed. Elsevier, Amsterdam, pp. 1–21.
Pettijohn, F.J, 1975. Sedimentary Rocks, 3rd ed. Harper and Row, New York, NY, 628 pp.
Pollington, A.D., Kozdon, R., Valley, J.W., 2011. Evolution of quartz cementation during burial of the Cambrian Mount Simon Sandstone, Illinois Basin: in situ microanalysis of $\delta^{18}O$. Geology 39, 1119–1122.
Pufahl, P.K., Hiatt, E.E., Kyser, T.K., 2010. Does the Paleoproterozoic Animikie Basin record the sulfidic ocean transition? Geology 38, 659–662.
Robert, F., Chaussidon, M., 2006. A palaeotemperature curve for the Precambrian oceans based on silicon isotopes in cherts. Nature 443, 969–972.
Schrag, D.P., Hampt, G., Murray, D.W., 1996. Pore fluid constraints on the temperature and oxygen isotopic composition of the glacial ocean. Science 272, 1930–1932.
Sharp, Z.D., Giletti, B.J., Yoder, H.S., 1991. Oxygen diffusion rates in quartz exchanged with CO_2. Earth Planet. Sci. Lett. 107, 339–348.
Simonson, B.M., 1985. Sedimentological constraints on the origins of Precambrian iron-formations. Geol. Soc. Am. Bull. 96, 244–252.
Simonson, B.M., 1987. Early silica cementation and subsequent diagenesis in arenites from four early Proterozoic iron formations of North America. J. Sed. Petrol. 57, 494–511.
Simonson, B.M., 2003. Origin and evolution of large Precambrian iron formations. In: Chan, M., Archer, A. (Eds.), Extreme Depositional Environments: Mega End Members in Geologic Time. Geological Society of America Special Paper, vol. 370, pp. 231–244.
Sippel, R.F., 1968. Sandstone petrology, evidence from luminescence petrography. J. Sed. Petrol. 38, 530–554.
Swart, P.K., 2000. The oxygen isotopic composition of interstitial waters: evidence for fluid flow and recrystallization in the margin of the Great Bahama Bank. In: Swart, P.K., Eberli, G.P., Malone, M.J., Sarg, J.F. (Eds.), Proc. ODP, Sci. Results, vol. 166. Ocean Drilling Program, College Station, TX, pp. 91–98.
Valaas Hyslop, E., Valley, J.W., Johnson, C.M., Beard, B.L., 2008. The effects of metamorphism on O and Fe isotope compositions in the Biwabik Iron formation, northern Minnesota. Contrib. Mineral. Petrol. 155, 313–328.
Valley, J.W., Kita, N.T., 2009. In situ oxygen isotope geochemistry by ion microprobe. In: Fayek, M. (Ed.), Secondary Ion Mass Spectrometry in the Earth Sciences: Gleaning the Big Picture from a Small Spot. Mineral. Assoc. Canada Short Course, vol. 41, pp. 19–63.
Williams, G.E., Schmidt, P.W., 2004. Paleomagnetism of the 1.88-Ga Sokoman Formation in the Schefferville–Knob Lake area, Québec, Canada, and implications for the genesis of iron oxide deposits in the central New Québec Orogen. Precambrian Res. 128, 167–188.
Winter, B.L., Knauth, L.P., 1992a. Stable isotope geochemistry of cherts and carbonates from the 2.0 Ga Gunflint iron formation – implications for the depositional setting, and the effects of diagenesis and metamorphism. Precambrian Res. 59, 283–313.
Winter, B.L., Knauth, L.P., 1992b. Stable isotope geochemistry of early Proterozoic carbonate concretions in the Animikie Group of the Lake Superior region: evidence for anaerobic bacterial processes. Precambrian Res. 54, 131–151.
Zajac, I.S., 1974. The Stratigraphy and Mineralogy of the Sokoman Formation in the Knob Lake area, vol. 220. Geological Survey of Canada Bulletin, Quebec and Newfoundland, 159 pp.